

Physical properties of noncentrosymmetric superconductor LaIrSi₃: A μ SR study

V. K. Anand,^{1,2,*} D. Britz,³ A. Bhattacharyya,^{1,3} D. T. Adroja,^{1,3,†} A. D. Hillier,¹ A. M. Strydom,³ W. Kockelmann,¹ B. D. Rainford,⁴ and K. A. McEwen⁵
¹*ISIS Facility, Rutherford Appleton Laboratory, Chilton, Didcot, Oxon, OX11 0QX, United Kingdom*
²*Helmholtz-Zentrum Berlin für Materialien und Energie, Hahn-Meitner Platz 1, D-14109 Berlin, Germany*
³*Highly Correlated Matter Research Group, Physics Department, University of Johannesburg, P.O. Box 524, Auckland Park 2006, South Africa*
⁴*Physics Department, University of Southampton, Southampton SO17 1BJ, United Kingdom*
⁵*Department of Physics and Astronomy and London Centre for Nanotechnology, University College London, Gower Street, London WC1E 6BT, United Kingdom*
 (Dated: July 25, 2014)

The results of heat capacity $C_p(T, H)$ and electrical resistivity $\rho(T, H)$ measurements down to 0.35 K as well as muon spin relaxation and rotation (μ SR) measurements on a noncentrosymmetric superconductor LaIrSi₃ are presented. Powder neutron diffraction confirmed the reported noncentrosymmetric body-centered tetragonal BaNiSn₃-type structure (space group $I4mm$) of LaIrSi₃. The bulk superconductivity is observed below $T_c = 0.72(1)$ K. The intrinsic $\Delta C_e/\gamma_n T_c = 1.09(3)$ is significantly smaller than the BCS value of 1.43, and this reduction is accounted by the α -model of BCS superconductivity. The analysis of the superconducting state $C_e(T)$ data by the single-band α -model indicates a moderately anisotropic order parameter with the s -wave gap $\Delta(0)/k_B T_c = 1.54(2)$ which is lower than the BCS value of 1.764. Our estimates of various normal and superconducting state parameters indicate a weakly coupled electron-phonon driven type-I s -wave superconductivity in LaIrSi₃. The μ SR results also confirm the conventional type-I superconductivity in LaIrSi₃ with a preserved time reversal symmetry and hence a singlet pairing superconducting ground state.

PACS numbers: 74.70.Dd, 74.25.Bt, 76.75.+i, 74.25.-q

I. INTRODUCTION

The noncentrosymmetric superconductors (NCSs) that allow mixing between spin-singlet and spin-triplet parity and exhibit exotic superconducting properties through the antisymmetric spin-orbit coupling (ASOC) are of great interest in the current research activities on superconductivity.¹ The NCSs lack inversion symmetry in their crystal structure that leads to a non uniform lattice potential and hence introduces an antisymmetric spin-orbit coupling. The ASOC removes the spin degeneracy of conduction band electrons, i.e., the spin-up and spin-down energy bands split and the two electrons forming a Cooper pair no longer belong to the *same* Fermi surface as in the conventional superconductors. An important consequence of Cooper pair formation by the electrons belonging to two *different* Fermi surfaces of spin-up and spin-down bands is that the the Cooper pair wave function of NCSs can no longer be classified by its parity as a pure spin-singlet or spin-triplet pairing, instead results in a parity mixing of spin singlet-triplet states.²⁻⁶ For centrosymmetric superconductors to which most of the known superconductors belong the spin-up and spin-down energy bands of the conduction electrons are degenerate when time reversal symmetry is conserved. The structural inversion symmetry thus has a key role in determining the superconducting properties and a number of unusual phenomena can be observed in such noncentrosymmetric materials.²⁻⁶

First such unusual superconducting behavior was

observed in heavy fermion superconductor CePt₃Si which crystallizes in a tetragonal structure (space group $P4mm$) that lacks a mirror symmetry along the c axis, and undergoes an antiferromagnetic transition below $T_N = 2.2$ K and becomes superconducting at the critical temperature $T_c = 0.75$ K that coexists with antiferromagnetic ordering.⁷ The upper critical field $H_{c2} \approx 5$ T is very high compared to the Pauli paramagnetic limiting field of ~ 1 T indicating a spin-triplet pairing.⁷ For a spin-singlet paring Pauli paramagnetic limiting is expected. On the other hand for a system without inversion symmetry spin-triplet pairing is not permitted.¹ These contradicting situation is accounted by mixed spin singlet-triplet states of order parameter.⁶ The irreducible representation point group for the tetragonal structure of CePt₃Si is C_{4v} in which Rashba-type ASOC exists that provides the key to understand the intriguing superconducting behavior of CePt₃Si.⁷⁻⁹ Following CePt₃Si many NCSs have been identified that present interesting superconducting properties including Li₂(Pd,Pt)₃B,^{10,11} CeRhSi₃,^{12,13} CeIrSi₃,¹⁴ CeCoGe₃,^{15,16} CeIrGe₃,¹⁷ LaNiC₂,¹⁸⁻²⁰ BaPtSi₃,²¹ (Rh,Ir)Ga₉,^{22,23} Mg₁₀Ir₁₉B₁₆,²⁴ Mo₃Al₂C,²⁵ LaRhSi₃,²⁶ Ca(Ir,Pt)Si₃,²⁷ Re₃W,²⁸ Nb_{0.18}Re_{0.12},²⁹ Re₆Zr,³⁰ La(Pd,Pt)Si₃,³¹ Ca₃Ir₄Ge₄³² etc.

The Ce-based NCSs CeRhSi₃, CeIrSi₃, CeCoGe₃ and CeIrGe₃ crystallize with BaNiSn₃-type tetragonal structure (space group $I4mm$) which lacks a mirror plane symmetry along the c axis and belongs to the same point group C_{4v} as CePt₃Si. Thus like CePt₃Si a Rashba-type ASOC is present in these CeMX₃ com-

pounds too, leading to exotic superconducting ground state in them.^{12–17,33–35} Like CePt₃Si they also exhibit heavy fermion behavior and undergo a long-range antiferromagnetic ordering, however, become superconducting only under the application of pressure.^{12–17,33–35} The above mentioned Ce-based NCSs are situated close to a magnetic quantum critical point making it difficult to explore the effects of ASOC and inversion symmetry breaking on superconductivity. Therefore nonmagnetic Rashba-type NCSs are essential for understanding the effect and extent of ASOC on the superconducting properties of these Ce-based NCSs. The reported nonmagnetic AMX_3 NCSs with BaNiSn₃-type tetragonal structure include BaPtSi₃ ($T_c = 2.25$ K), LaRhSi₃ [$T_c = 2.16(8)$ K], CaIrSi₃ ($T_c = 3.6$ K), CaPtSi₃ ($T_c = 2.3$ K), LaPdSi₃ [$T_c = 2.65(5)$ K] and LaPtSi₃ [$T_c = 1.52(6)$ K].^{21,26,27,31} All these nonmagnetic NCSs behave like conventional s -wave superconductor without any noticeable effect of absence of inversion symmetry in their crystal structure. Nevertheless, being isostructural they provide a direct comparison with Ce MX_3 NCSs and the investigations of these nonmagnetic NCSs connote the role of $4f$ moments in Ce NCSs. One important difference between the Ce MX_3 NCSs and these nonmagnetic NCSs is that Ce MX_3 exhibit superconductivity only at high pressures whereas these nonmagnetic NCSs superconduct at ambient pressure. This difference may have its origin in magnetic pairing in Ce NCSs in contrast to phonon mediated superconductivity in these nonmagnetic NCSs.

Theoretically the Rashba-type ASOC has been studied extensively and is favored for the investigations of NCSs, therefore compounds with tetragonal BaNiSn₃-type structure represents an important class of non-centrosymmetric materials. Continuing our work on BaNiSn₃-type structured materials we have performed a comprehensive study of superconducting and normal state properties of NCS LaIrSi₃ using heat capacity C_p and electrical resistivity ρ versus temperature T measurements down to 0.35 K, and muon spin relaxation and rotation (μ SR) measurements down to 50 mK. The reported noncentrosymmetric body-centered tetragonal BaNiSn₃-type structure of LaIrSi₃ is confirmed by our room temperature powder XRD and neutron diffraction. Superconductivity in LaIrSi₃ was reported about 30 years ago with T_c between 1.9–2.7 K based on resistivity measurement.^{36,37} In a recent study Okuda et al. reported a superconducting transition at $T_c = 0.77$ K from the heat capacity measurement on LaIrSi₃.³³ Okuda et al. also carried out de Haas-van Alphen (dHvA) effect study and found that as a result of Rashba-type ASOC the Fermi surface of LaIrSi₃ splits into two Fermi surfaces (spin-up and spin-down energy bands) which are separated by about 1000 K.³³ In our recent investigations of superconducting properties of NCS LaRhSi₃ we found a conventional type-I superconductivity with preserved time reversal symmetry, however, with an unusual exponential evolution of Sommerfeld coefficient γ with magnetic field which could be due to the reinforcement

of ASOC with magnetic field.²⁶ Therefore in view of unusual behavior of LaRhSi₃ and strong effect of ASOC in LaIrSi₃ revealed by de Haas-van Alphen (dHvA) effect study, it was felt necessary to investigate the superconducting properties of LaIrSi₃ in detail, which we present in this paper.

Our $C_p(T)$ data confirm bulk superconductivity in LaIrSi₃ below $T_c = 0.72(1)$ K in agreement with the report by Okuda et al.³³ However, the $\rho(T)$ exhibits superconductivity at a higher $T_c = 1.45$ K apparently due to filamentary nonbulk superconductivity. The normal-state ρ is metallic and well described by the Bloch-Grüneisen model of resistivity for $T \geq 1.6$ K. The low- T normal-state $C_p(T)$ gives electronic coefficient $\gamma_n = 4.60(2)$ mJ/molK² and density of states at Fermi energy $\mathcal{D}(E_F) = 1.95(1)$ states/eV f.u. for both spin directions, where f.u. stands for formula unit. A sharp jump is observed at $T_c = 0.72(1)$ K in electronic heat capacity $C_e(T)$ with $\Delta C_e/\gamma_n T_c = 1.09(3)$ which is smaller than the BCS expected value of 1.43. Within the single-band picture the reduced value of $\Delta C_e/\gamma_n T_c$ can be attributed to anisotropic energy gap in LaIrSi₃. We have analyzed the superconducting state electronic heat capacity data by α -model of BCS superconductivity^{38–40} which suggests that the s -wave order parameter of LaIrSi₃ is anisotropic in momentum space with an energy gap $\Delta(0)/k_B T_c = 1.54(2)$. We have estimated various normal and superconducting state parameters that indicate a weak-coupling type-I BCS superconductivity in dirty limit. Our μ SR investigations also confirm type-I superconductivity in LaIrSi₃. Further, μ SR results also show that the time-reversal symmetry is preserved as is expected for a conventional s -wave singlet pairing superconductivity. No evidence of parity mixing is observed as one would have expected in view of splitting of spin-up and spin-down energy bands revealed by dHvA study.³³

II. EXPERIMENTAL DETAILS

A polycrystalline sample of LaIrSi₃ was prepared by the standard arc melting of stoichiometric mixture of high purity elements (La: 99.9%, Ir: 99.99%, Si 99.999%) on a water cooled copper hearth under the titanium gettered inert argon atmosphere with several flips to ensure homogeneity. The arc melted sample was further heat treated at 900 °C for a week under the dynamic vacuum. The crystal structure was determined by the powder x-ray diffraction (XRD) using Cu K α radiation. The heat capacity measurements were performed by the relaxation method with a physical properties measurement system (PPMS, Quantum Design, Inc.). The electrical resistivity measurements were performed by the standard four probe ac technique using the PPMS. Temperatures down to 0.35 K were attained by a ³He attachment to PPMS.

Powder neutron diffraction (ND) measurement was performed at room temperature using the ROTAX diffractometer at the ISIS facility of the Rutherford Ap-

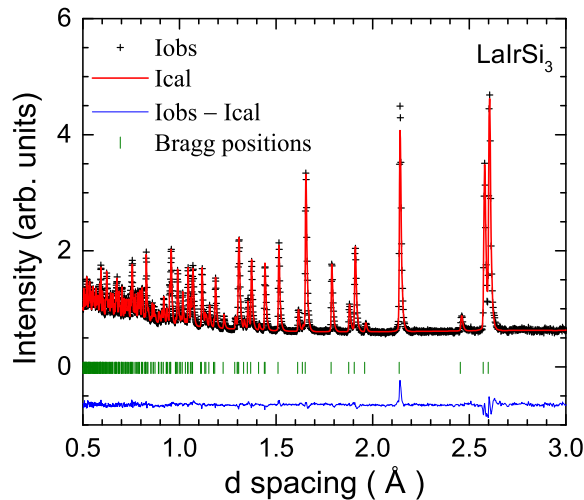


FIG. 1. (Color online) Powder neutron diffraction pattern of LaIrSi_3 recorded at room temperature. The solid line through the experimental points is the Rietveld refinement profile calculated for noncentrosymmetric body-centered tetragonal BaNiSn_3 -type structure (space group $I4mm$). The short vertical bars indicate the Bragg peak positions. The lowermost curve represents the difference between the experimental and calculated intensities.

pleton Laboratory, Didcot, U.K. The μSR measurements were carried out using the μSR spectrometer at the ISIS facility with the detectors in both longitudinal and transverse configurations. A high purity silver plate was used to mount the sample which gives only a nonrelaxing muon signal. The powdered sample was mounted on silver plate using diluted GE varnish that was covered with kapton film. Temperatures down to 50 mK were achieved by cooling the sample in a dilution refrigerator. Correction coils were used to counter-effect the stray fields at the sample position to within $1 \mu\text{T}$.

III. CRYSTALLOGRAPHY

The room temperature powder XRD data were analyzed by structural Rietveld refinement using the program Fullprof.⁴¹ The refinement confirmed the reported BaNiSn_3 -type tetragonal structure (space group $I4mm$) of LaIrSi_3 and revealed the single phase nature of sample without any trace of impurity phase. The single phase nature of whole bulk of sample is further inferred from the Rietveld refinement of room temperature powder neutron diffraction data that was performed using the program GSAS.⁴² Neutron diffraction pattern and refinement profile for noncentrosymmetric body-centered tetragonal BaNiSn_3 -type structure are shown in Fig. 1. While refining no improvement in the fit quality was observed upon refining the occupancies of atomic positions, and within the error bar the atomic occupancies were found to be unity, therefore in the final refinement we fixed the occupancies to unity. The crystallographic pa-

TABLE I. Crystallographic parameters obtained from the structural Rietveld refinement of room temperature powder neutron diffraction data of LaIrSi_3 . Profile reliability factor $R_p = 2.60\%$ and weighted profile R -factor $R_{wp} = 2.33\%$.

Structure	BaNiSn ₃ -type tetragonal				
Space group	<i>I4mm</i> (No. 107)				
Lattice parameters					
<i>a</i> (Å)	4.2784(3)				
<i>c</i> (Å)	9.8308(7)				
<i>V</i> _{cell} (Å ³)	179.95(4)				
<u>Atomic coordinates</u>					
Atom	Wyckoff position	<i>x</i>	<i>y</i>	<i>z</i>	<i>U</i> _{iso} (Å ²)
La	2a	0	0	0	0.0008(3)
Ir	2a	0	0	0.6554(2)	0.0021(3)
Si1	2a	0	0	0.4140(3)	0.0003(3)
Si2	4b	0	1/2	0.2624(2)	0.0033(3)

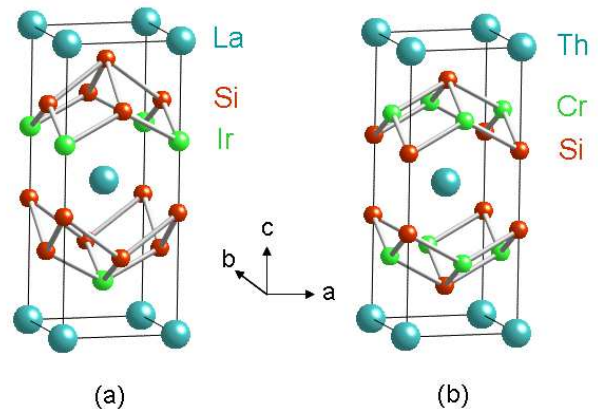


FIG. 2. (Color online) Comparison of (a) BaNiSn_3 -type non-centrosymmetric body-centered tetragonal structure ($I4mm$) of LaIrSi_3 and (b) ThCr_2Si_2 -type body-centered tetragonal crystal structure ($I4/mmm$).

rameters obtained from the refinement of powder neutron diffraction are listed in Table I. Both ND and XRD data gave similar crystallographic parameters and agree well with the literature values.^{36,43}

The BaNiSn_3 -type body-centered tetragonal structure (space group $I4mm$) of LaIrSi_3 is illustrated in Fig. 2 and is compared with the common ThCr_2Si_2 -type body-centered tetragonal structure (space group $I4/mmm$). Like ThCr_2Si_2 -type structure the BaNiSn_3 -type structure is also a layered structure and a ternary derivative of BaAl_4 -type structure.⁴⁴ The R (La, Th) atoms occupy identical positions in both structures and form body-centered tetragonal sublattice. However, they differ in the positions of T (Ir, Cr) and Si atoms. The T atoms form square sublattice in ab plane in both the structures but they are rotated by 45° in ab plane with respect to each other. Further, in ThCr_2Si_2 -type structure all the Si atoms occupy a single crystallographic site whereas in BaNiSn_3 -type structure the Si atoms occupy

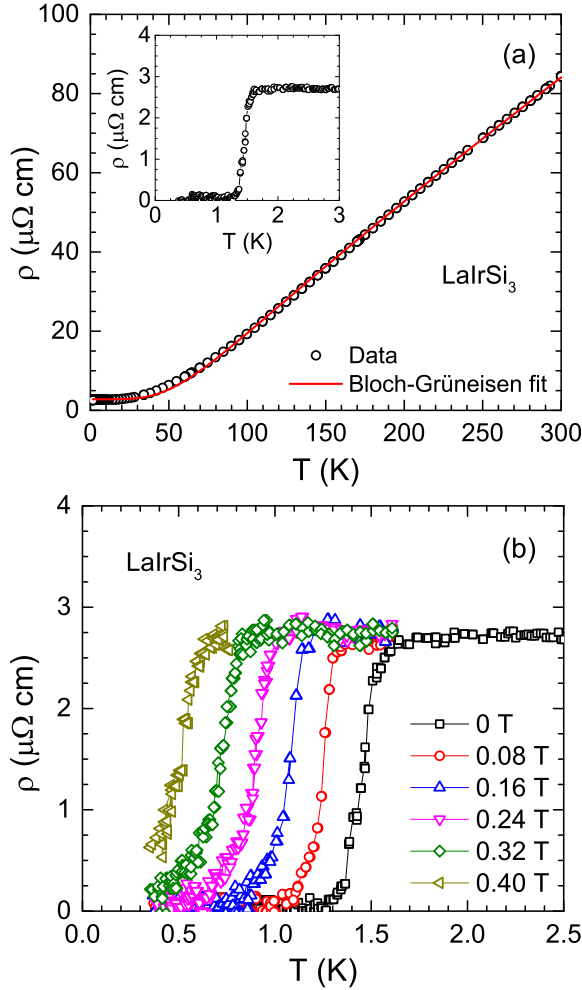


FIG. 3. (Color online) (a) Electrical resistivity ρ of LaIrSi_3 as a function of temperature T for $1.6\text{ K} \leq T \leq 300\text{ K}$ measured in applied magnetic field $H = 0$. The red solid curve is a fit of $\rho(T)$ data by the Bloch-Grüneisen model. Inset: Expanded view of $\rho(T)$ below 3 K to show the superconductivity. (b) The $\rho(T)$ of LaIrSi_3 for $0.35\text{ K} \leq T \leq 2.5\text{ K}$ showing the superconducting transitions for different values of H .

two different sites and hence the stacking order of T and Si layers along the c axis is different in the two structures. The structural difference in the two structures is evident from Fig. 2. It is seen that the BaNiSn_3 -type structure is not symmetric about the R plane and there is a loss of mirror plane along the c axis in BaNiSn_3 -type structure which is present in the ThCr_2Si_2 -type structure. The ThCr_2Si_2 -type structure is centrosymmetric whereas the BaNiSn_3 -type structure is noncentrosymmetric.

IV. ELECTRICAL RESISTIVITY

The electrical resistivity ρ of LaIrSi_3 as a function of T for $0.35\text{ K} \leq T \leq 300\text{ K}$ measured at applied magnetic field $H = 0$ is shown in Fig. 3(a). A metallic behavior is

inferred from the T dependence of ρ , the ρ decreases with decreasing T , becomes nearly constant in the low- T limit below 25 K and undergoes a sharp transition to a zero resistance state due to the occurrence of superconductivity. It is seen that onset of superconductivity takes place at $T_{c\text{onset}} \approx 1.6\text{ K}$ and zero resistivity state is reached at $T_{c0} \approx 1.3\text{ K}$. Thus a $T_c = 1.45\text{ K}$ (defined as the mid point of the transition) is obtained from the resistivity data. The $\rho(T)$ data at various H for $0 \leq H \leq 0.4\text{ T}$ are shown in Fig. 3(b). It is seen that the T_c decreases with increasing H , at $H = 0.32\text{ T}$, T_c reduces to 0.70 K from 1.45 K at $H = 0$.

From Fig. 3(a) the residual resistivity before entering the superconducting state is $\rho_0 = 2.7\text{ }\mu\Omega\text{ cm}$ and a residual resistivity ratio $\text{RRR} \equiv \rho(300\text{ K})/\rho(1.6\text{ K}) \approx 31$. The low value of ρ_0 and high value of RRR indicate good sample quality. In the normal state, the $\rho(T \geq 1.6\text{ K})$ data are well described by the Bloch-Grüneisen (BG) model of resistivity due to the scattering of conduction electrons by longitudinal acoustic lattice vibrations.⁴⁵ We fitted our normal-state $\rho(T)$ data by

$$\rho(T) = \rho_0 + \rho_{\text{BG}}, \quad (1)$$

where

$$\rho_{\text{BG}}(T/\Theta_R) = 4\mathcal{R} \left(\frac{T}{\Theta_R} \right)^5 \int_0^{\Theta_R/T} \frac{x^5}{(e^x - 1)(1 - e^{-x})} dx, \quad (2)$$

represents the BG resistivity. The Θ_R is the Debye temperature from the resistivity data and \mathcal{R} is a material-dependent prefactor.

Our fit of $\rho(T)$ data in $1.6\text{ K} \leq T \leq 300\text{ K}$ by BG model is shown by the solid red curve in Fig. 3(a) where we used an analytic Padé approximant fitting function for ρ_{BG} from Ref. 46. From the fitting of $\rho(T)$ data we obtain $\rho_0 = 2.81(2)\text{ }\mu\Omega\text{ cm}$, $\Theta_R = 331(2)\text{ K}$ and $\mathcal{R} = 95.7\text{ }\mu\Omega\text{ cm}$. Further details about the fitting of $\rho(T)$ by the Bloch-Grüneisen model of resistivity can be found in Refs. 46 and 47.

V. HEAT CAPACITY

The heat capacity C_p of LaIrSi_3 as a function of T for $0.35\text{ K} \leq T \leq 300\text{ K}$ measured at $H = 0$ is shown in Fig. 4(a). As shown in the inset a sharp jump is observed in C_p due to the superconducting transition at $T_c = 0.72(1)\text{ K}$. The observation of such a sharp jump in $C_p(T)$ indicates the occurrence of bulk superconductivity in LaIrSi_3 . The $C_p(T)$ data measured at different magnetic fields are shown in Fig. 4(b). It is seen that the jump ΔC_p in C_p as well as T_c decrease with the increasing H . The T_c is found to decrease to $0.44(2)\text{ K}$ at $H = 5.0\text{ mT}$ from its value of $T_c = 0.72(1)\text{ K}$ at $H = 0$, and is suppressed to a temperature below 0.35 K by a field of $H = 7.0\text{ mT}$. The suppression of T_c with H for $C_p(T, H)$ is very different from that observed for

the $\rho(T, H)$ data above where superconductivity survives even at an applied field of 0.4 T.

The low temperature normal state heat capacity data are well described by $C_p(T) = \gamma_n T + \beta T^3$. The normal state Sommerfeld electronic heat capacity coefficient γ_n is estimated by fitting the normal-state $C_p(T)$ data measured at $H = 0$ (in $0.75 \text{ K} \leq T \leq 3.8 \text{ K}$) and at $H = 10.0 \text{ mT}$ (in $0.35 \text{ K} \leq T \leq 0.9 \text{ K}$) simultaneously. The simultaneous linear fit of $C_p(T)/T$ versus T^2 by $C_p(T)/T = \gamma_n + \beta T^2$ in $0.35 \text{ K} \leq T \leq 3.8 \text{ K}$ yield $\gamma_n = 4.60(2) \text{ mJ/mol K}^2$ and $\beta = 0.17(1) \text{ mJ/mol K}^4$. The coefficient β according to the relation⁴⁸ $\Theta_D = (12\pi^4 R p / 5\beta)^{1/3}$, where R is the molar gas constant and $p = 5$ is the number of atoms per formula unit (f.u.), gives the Debye temperature $\Theta_D = 385(8) \text{ K}$. The experimental $C_p(T = 300 \text{ K}) \approx 106 \text{ J/mol K}$ does not reach the Dulong-Petit high- T limit of the lattice heat capacity $C_V = 3pR = 15R = 124.7 \text{ J/mole K}$.

The coefficient γ_n can be used to estimate the density of states at the Fermi level $\mathcal{D}(E_F)$ which according to the relation⁴⁸ $\gamma_n = (\pi^2 k_B^2 / 3) \mathcal{D}(E_F)$ gives $\mathcal{D}(E_F) = 1.95(1) \text{ states/eV f.u.}$ for both spin directions. This $\mathcal{D}(E_F)$ contains the quasi-particle mass enhancement by many-body electron-phonon interaction and is related to the bare density of states $\mathcal{D}_{\text{band}}(E_F)$ by⁴⁹ $\mathcal{D}(E_F) = (1 + \lambda_{e-\text{ph}}) \mathcal{D}_{\text{band}}(E_F)$, where $\lambda_{e-\text{ph}}$ is the electron-phonon coupling constant that can be estimated from Θ_D and T_c using the McMillan's relation⁵⁰

$$\lambda_{e-\text{ph}} = \frac{1.04 + \mu^* \ln(\Theta_D / 1.45 T_c)}{(1 - 0.62\mu^*) \ln(\Theta_D / 1.45 T_c) - 1.04}. \quad (3)$$

Here μ^* is the repulsive screened Coulomb parameter usually assigned as $\mu^* = 0.13$. For LaIrSi_3 we have $T_c = 0.72 \text{ K}$ and $\Theta_D = 385 \text{ K}$ which together with $\mu^* = 0.13$, according to Eq. (3) gives $\lambda_{e-\text{ph}} = 0.41$. The small value of $\lambda_{e-\text{ph}}$ implies a weak-coupling superconductivity in LaIrSi_3 . This value of $\lambda_{e-\text{ph}}$ combined with $\mathcal{D}(E_F) = 1.95(1) \text{ states/eV f.u.}$ for both spin directions gives $\mathcal{D}_{\text{band}}(E_F) = 1.38(1) \text{ states/eV f.u.}$ for both spin directions. The effective mass m^* of the quasi-particle can be obtained from $m^* = (1 + \lambda_{e-\text{ph}}) m_{\text{band}}^*$ which gives $m^* = 1.41 m_e$ assuming the effective band mass $m_{\text{band}}^* = m_e$, the free electron mass.

The density of states and hence γ_n can be further used to estimate the Fermi velocity v_F which is related to $\mathcal{D}(E_F)$ by⁴⁸ $v_F = (\pi^2 \hbar^3 / m^* n e^2 V_{\text{f.u.}}) \mathcal{D}(E_F)$, where \hbar is Planck's constant divided by 2π and $V_{\text{f.u.}} = V_{\text{cell}}/2$ is the volume per formula unit. We thus estimate $v_F = 9.49 \times 10^7 \text{ cm/s}$ for LaIrSi_3 using the above estimated $\mathcal{D}(E_F)$ and m^* . The v_F together with ρ_0 can be used to estimate the mean free path ℓ , as $\ell = v_F \tau$ and the mean free scattering time $\tau = m^* / n e^2 \rho_0$, with the conduction carrier density $n = m^* v_F^3 / 3\pi^2 \hbar^3$ assuming a spherical Fermi surface.⁴⁸ Combining all these

$$\ell = 3\pi^2 \left(\frac{\hbar}{e^2 \rho_0} \right) \left(\frac{\hbar}{m^* v_F} \right)^2. \quad (4)$$

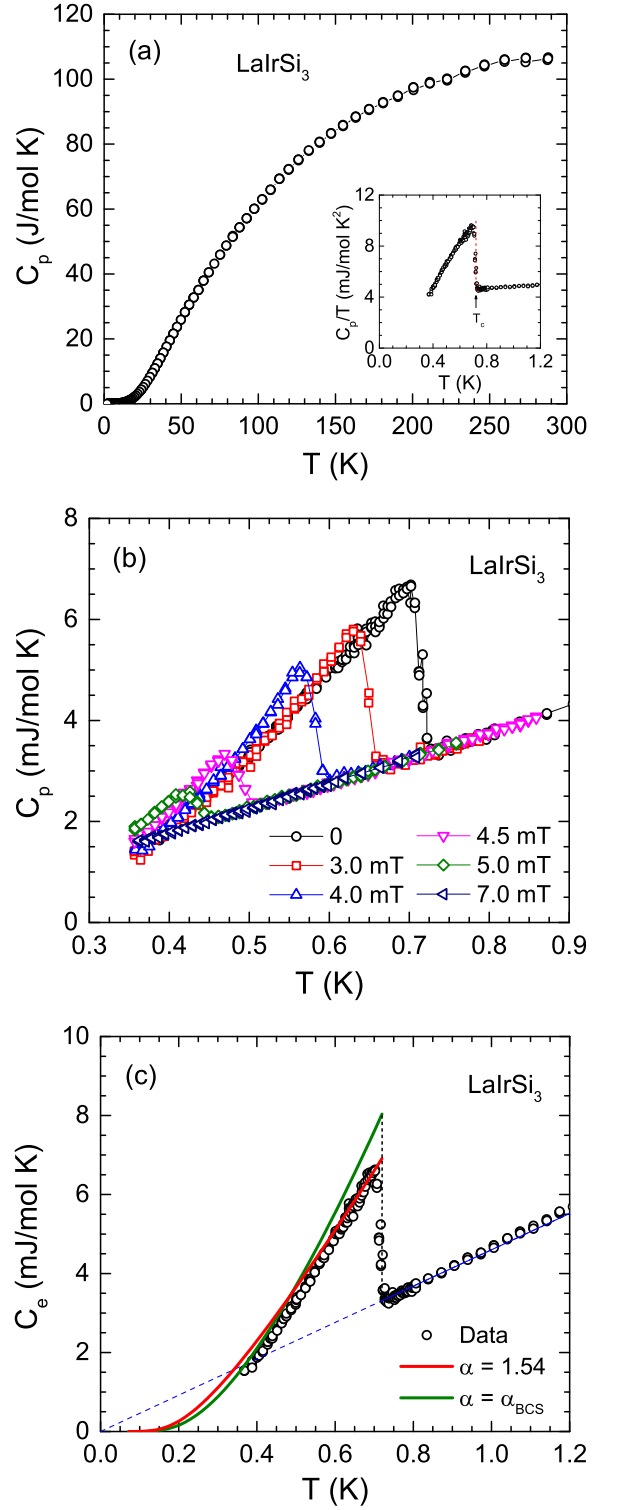


FIG. 4. (Color online) (a) Heat capacity C_p of LaIrSi_3 as a function of temperature T for $1.8 \text{ K} \leq T \leq 300 \text{ K}$ measured in zero magnetic field. Inset: C_p/T vs. T for $0.35 \text{ K} \leq T \leq 1.2 \text{ K}$. The dotted red line mark the superconducting transition temperature T_c . (b) $C_p(T)$ for $0.35 \text{ K} \leq T \leq 0.9 \text{ K}$ measured in different applied magnetic fields. (c) Electronic contribution C_e to zero field heat capacity as a function of temperature T . The solid red curve is the theoretical prediction of the α -model for $\alpha = \Delta(0)/k_B T_c = 1.54$. The BCS prediction for the $\alpha_{\text{BCS}} = 1.764$ is also shown for comparison.

which for $\rho_0 = 2.7 \mu\Omega\text{cm}$ and above estimated v_F and m^* gives $\ell = 33.7 \text{ nm}$.

VI. SUPERCONDUCTING STATE PROPERTIES

The electronic contribution to the heat capacity $C_e(T)$ after subtracting off the phonon contribution from the measured $C_p(T)$ data, i.e. $C_e(T) = C_p(T) - \beta T^3$ is shown in Fig. 4(c) clearly showing the sharp jump in C_e at T_c . The jump ΔC_e in C_e at T_c is found to be $\Delta C_e = 3.6(1) \text{ mJ/molK}$ corresponding to the vertical dotted line at T_c in Fig. 4(c). This gives $\Delta C_e/\gamma_n T_c = 1.09(3)$ for $\gamma_n = 4.60(2) \text{ mJ/molK}^2$ and $T_c = 0.72(1) \text{ K}$ which is significantly smaller than the BCS value of $\Delta C_e/\gamma_n T_c = 1.43$ in the weak-coupling limit.⁵¹ Presence of a residual heat capacity due to small impurity/nonsuperconducting phase can lead to a reduced $\Delta C_e/\gamma_n T_c$. However, in view of the fact that the jump in $C_e(T)$ at the superconducting transition is very sharp, the entire sample seems to be superconducting without any residual γ , which in turn suggests that the reduction in $\Delta C_e/\gamma_n T_c$ is intrinsic. In a single-band model, such a reduction can be caused by the presence of anisotropic superconducting energy gap (order parameter) in momentum space.³⁸ That the reduction in $\Delta C_e/\gamma_n T_c$ is intrinsic will be clear from our analysis of the superconducting state data by single-band α -model of BCS superconductivity^{38–40} below which is applicable to the system with $\Delta C_e/\gamma_n T_c \neq 1.43$.

In the so-called α -model of BCS superconductivity in order to fit the superconducting state thermodynamic data, the $\alpha_{\text{BCS}} \equiv \Delta(0)/k_B T_c = 1.764$ is replaced by a variable α .^{38,39} The α is determined from the jump ΔC_e at T_c according to the relation³⁸

$$\frac{\Delta C_e(T_c)}{\gamma_n T_c} = 1.426 \left(\frac{\alpha}{\alpha_{\text{BCS}}} \right)^2 \quad (5)$$

which for $\Delta C_e/\gamma_n T_c = 1.09(3)$ gives $\alpha = 1.54(2)$. This value of α is significantly smaller than the BCS value of 1.764. The temperature dependence of α -model superconducting state heat capacity $C_e(T)$ calculated for $\alpha = 1.54$ is shown by the solid red curve in Fig. 4(c) together with that of BCS prediction for $\alpha = \alpha_{\text{BCS}}$. A reasonable agreement is observed between the α -model prediction and the superconducting state $C_e(T)$ data which supports the applicability of α -model and in turn indicates that the s -wave order parameter of LaIrSi₃ is anisotropic in momentum space. The details about the fitting of $C_e(T)$ data by α -model of BCS superconductivity can be found in Refs. 38 and 52. The lack of perfect agreement between the α -model prediction and the experimental data may indicate that the anisotropy of gap is not well accounted, as the simplified α -model does not account for the energy dependence of the gap function or for a complex Δ .

The thermodynamic critical field H_c is estimated from the zero-field $C_e(T)$ data by integrating the en-

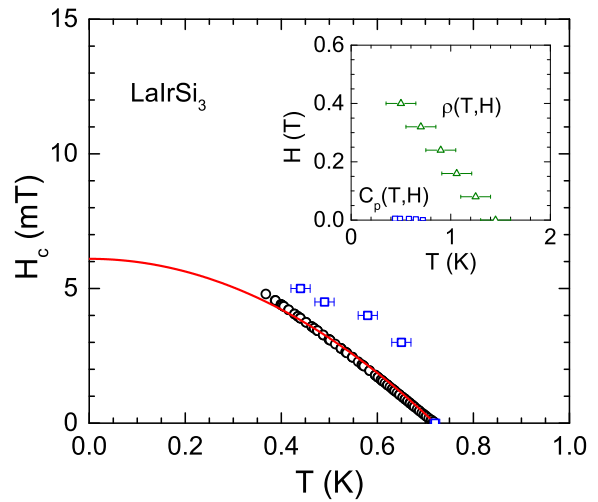


FIG. 5. (Color online) Thermodynamic critical field H_c of LaIrSi₃ as a function of temperature T obtained from the experimental electronic heat capacity $C_e(T)$ data. The H dependent T_c obtained from the heat capacity $C_p(T, H)$ data in Fig. 4(b) are also shown by open squares. The solid line represents the parabolic fit to $H_c(T) = H_c(0)[1 - (T/T_c)^2]$ as discussed in the text. Inset: H - T phase diagram obtained from the electrical resistivity $\rho(T, H)$ in Fig. 3(b) together with $T_c(H)$ from $C_p(T, H)$.

tropy difference between the superconducting and normal states,^{51,53} $H_c^2(T) = 8\pi \int_T^{T_c} [S_{\text{en}}(T') - S_{\text{es}}(T')] dT'$, where S_{en} and S_{es} are the electronic entropy of normal and superconducting states, respectively, with $S_e(T') = \int_0^{T'} [C_e(T'')/T''] dT''$. The $H_c(T)$ obtained from the zero-field $C_e(T)$ this way is shown in Fig. 5. The T dependence of H_c can be approximated to the conventional relation $H_c(T) = H_c(0)[1 - (T/T_c)^2]$, which gives $H_c(0) = 6.10(3) \text{ mT}$. The solid red curve in Fig. 5 represents the fit of $H_c(T)$ data with this expression.

The experimental $H_c(0)$ obtained so is somewhat higher than the theoretical $H_c(0)$ which for α -model is given by³⁸

$$\frac{H_c(0)}{(\gamma_n v T_c^2)^{1/2}} = \sqrt{\frac{6}{\pi}} \alpha \approx 1.382 \alpha, \quad (6)$$

where the Sommerfeld coefficient per unit volume γ_{nV} is in units of $\text{erg/cm}^3 \text{ K}^2$. From this relation for $\alpha = 1.54$ we obtain $H_c(0) = 4.5 \text{ mT}$ which is little lower than the $H_c(0) = 6.10(3) \text{ mT}$ obtained above. Even for $\alpha_{\text{BCS}} = 1.764$, Eq. (6) gives a lower $H_c(0) = 5.1 \text{ mT}$. The reason for this discrepancy between the experimental and theoretical values of $H_c(0)$ is not clear. We suspect that this might be the result of a nonspherical/anisotropic Fermi surface in LaIrSi₃ which is not properly accounted by Eq. (6).

Further, as can be seen from Fig. 5, the $H_c(T)$ obtained from the zero-field $C_e(T)$ data and H - T phase diagram determined from the H dependent T_c from $C_p(T, H)$ data

in Fig. 4(b) both give very low critical fields. For a type-II superconductivity the $T_c(H)$ obtained from $C_p(T, H)$ gives the upper critical field H_{c2} that is usually much higher than the thermodynamic critical field, which is not the present case. The fact that $H_{c2}(T)$ is close to $H_c(T)$ may suggest a type-I superconductivity in LaIrSi₃ or a type 1.5 behavior that may arise from the presence of split spin-up and spin-down energy bands similar to what has been observed in two-band superconductor MgB₂.⁵⁴

The H dependent T_c from $\rho(T, H)$ data in Fig. 3(b) is shown in the inset of Fig. 5 which show very different behavior than the $T_c(H)$ from $C_p(T, H)$ data. This is consistent with the observation of different T_c 's in resistivity and heat capacity measurements in zero field mentioned above, apparently due to the filamentary/surface superconductivity that sets in at a temperature higher than the bulk superconductivity. Our estimate of Ginzburg-Landau parameter κ below gives $\kappa = 0.55$ which suggests a type-I behavior. Usually for a type-I superconductor one do not expect a filamentary or surface superconductivity. However, surface superconductivity is predicted for a type-I superconductor with κ values between $1/\sqrt{2}$ and $1/2.39$.^{55,56} Indeed our estimated κ lies between these limits and we can expect a surface superconductivity in LaIrSi₃. The critical field associated with the surface superconductivity is given by^{55,56} $H_{c3} = 2.39 \kappa H_c$, accordingly for LaIrSi₃ we estimate $H_{c3} = 8.0$ mT which is much smaller than the observed upper critical field from resistivity measurement (inset of Fig. 5). Thus the observed $T_c(H)$ from $\rho(T, H)$ could not be understood to arise from surface superconductivity. The reason for such high critical field in resistivity measurement of LaIrSi₃ is not clear. The type I superconductor LaPdSi₃ was also found to exhibit a higher critical field in resistivity measurement compared to that in heat capacity.³¹ In a recent study N. Kimura et al.⁵⁷ found a similar high critical field from the resistivity measurement on type-I superconductor LaRhSi₃ where they argue that this behavior may be a common feature in noncentrosymmetric superconductors. However, we are not aware of any theoretical discussion of this aspect of noncentrosymmetric superconductors, and this hypothesis needs to be tested theoretically.

Our estimate of the superconducting London penetration depth in the clean limit at $T = 0$, $\lambda_L(0)$ from v_F using the relation⁵¹

$$\lambda_L(0)^2 = \frac{m^* c^2}{4\pi n e^2} = \frac{3\pi c^2 \hbar^3}{4m^* e^2 v_F^3}, \quad (7)$$

where c is the speed of light in vacuum, gives $\lambda_L(0) = 25.9$ nm for $v_F = 9.49 \times 10^7$ cm/s. The BCS coherence length ξ_0 can be obtained from v_F and energy gap $\Delta(0)$ which for the α -model is given by³⁸

$$\xi_0 = \frac{\hbar v_F}{\pi \Delta(0)} = \left(\frac{1}{\pi \alpha} \right) \frac{\hbar v_F}{k_B T_c}. \quad (8)$$

This gives $\xi_0 = 2081$ nm for $\alpha = 1.54$ and $v_F = 9.49 \times 10^7$ cm/s. We see that ξ_0 is much larger than

TABLE II. Measured and derived superconducting and relevant normal state parameters for the noncentrosymmetric superconductor LaIrSi₃.

T_c (K)	0.72(1)
γ_n (mJ/mol K ²)	4.60(2)
Θ_D (K)	385(8)
λ_{e-ph}	0.41
ΔC_e (mJ/mol K)	3.6(1)
$\Delta C_e / \gamma_n T_c$	1.09(3)
$\alpha \equiv \Delta(0) / k_B T_c$ (from $\Delta C_e / \gamma_n T_c$)	1.54(2)
$\Delta(0) / k_B$ (K)	1.11
$H_c(T = 0)$ (mT)	6.10(3)
κ_{GL}	0.55
$\xi(0)$ (nm)	373
ξ_0 (nm)	2081
ℓ (nm)	33.7
$\lambda_L(0)$ (clean limit) (nm)	25.9
$\lambda_{eff}(0)$ (dirty limit) (nm)	205

the above estimated mean free path $\ell = 33.7$ nm, $\ell / \xi_0 \approx 0.016 \ll 1$, suggesting that the superconductivity in LaIrSi₃ is in the dirty-limit. In the dirty limit, the Ginzburg-Landau parameter $\kappa_{GL} = 0.715 \lambda_L(0) / \ell$,⁵¹ which gives $\kappa_{GL} = 0.55 < 1/\sqrt{2}$, as expected for a type-I superconductivity. This value of κ_{GL} is close to the value obtained using the dirty-limit relation for a fully gapped (isotropic) superconductor,⁵⁸ $\kappa_{GL} = 7.49 \times 10^3 \rho_0 \sqrt{\gamma_{nV}}$, with ρ_0 in Ω cm, which gives $\kappa_{GL} = 0.59$. Both estimates of κ_{GL} consistently indicate a type-I superconductivity in LaIrSi₃.

The effective magnetic penetration depth λ_{eff} can be estimated using the dirty limit relation⁵¹

$$\lambda_{eff}(0) = \lambda_L(0) \sqrt{1 + \frac{\xi_0}{\ell}} \quad (\text{dirty limit}). \quad (9)$$

which gives $\lambda_{eff}(0) = 205$ nm. Then using the relation $\kappa_{GL} = \lambda_{eff}(0) / \xi(0)$ we estimate the Ginzburg-Landau coherence length $\xi(0)$ which for $\kappa_{GL} = 0.55$ yields $\xi(0) = 373$ nm. The measured and derived superconducting parameters of LaIrSi₃ are listed in Table II.

VII. MUON SPIN RELAXATION AND ROTATION

The time evolution of muon spin relaxation in zero field (ZF) is shown in Fig. 6 for both at T above and below the bulk T_c . It is evident from the ZF μ SR spectra that there is no noticeable change in the relaxation rates at 1.0 K ($> T_c$) and 0.05 K ($< T_c$). This indicates that the time reversal symmetry remains preserved upon entering the superconducting state. The ZF μ SR spectra are best described by the Gaussian Kubo-Toyabe function,

$$G_z(t) = A_0 \left[\frac{1}{3} + \frac{2}{3} (1 - \sigma^2 t^2) e^{-\sigma^2 t^2 / 2} \right] e^{-\lambda t} + A_{BG}, \quad (10)$$

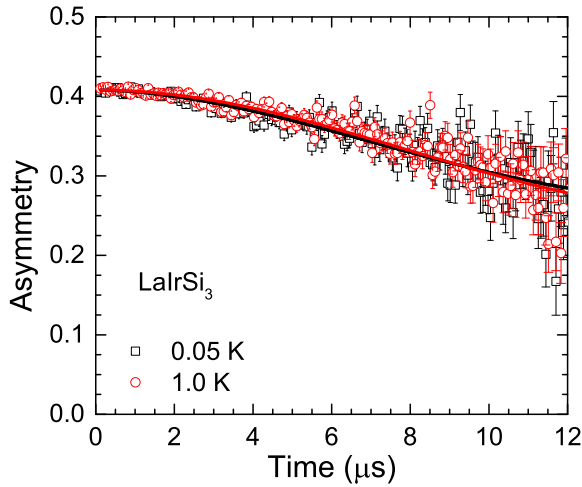


FIG. 6. (Color online) Zero field μ SR spectra of LaIrSi₃ measured in longitudinal geometry at temperatures above (1.0 K) and below (0.05 K) the superconducting T_c . The solid curves are the fits by Gaussian Kubo-Toyabe function in Eq. (10).

where A_0 is the initial asymmetry, σ and λ are the depolarization rates, and A_{BG} is the time-independent background contribution. σ accounts for the Gaussian distribution of static fields from nuclear moments [the local field distribution width $\langle H_\mu \rangle = \sigma/\gamma_\mu$ with muon gyromagnetic ratio $\gamma_\mu = 135.53$ MHz/T] and λ accounts for the electronic moments. The fits of μ SR spectra in Fig. 6 by the decay function in Eq. (10) give $\sigma = 0.074(1) \mu s^{-1}$ and $\lambda = 0.009(3) \mu s^{-1}$ at 1.0 K and $\sigma = 0.074(1) \mu s^{-1}$ and $\lambda = 0.011(2) \mu s^{-1}$ at 0.05 K. The fits are shown by solid red curve in Fig. 6. Since within the error bars both σ and λ at $T < T_c$ and $T > T_c$ are similar, there is no evidence of time reversal symmetry breaking in LaIrSi₃.

The time evolution of muon spin rotation in transverse field (TF) is shown in Fig. 7. The TF muon spin precession signals were collected on field cooled sample at different applied fields both above (1.0 K) and below (0.05 K) T_c . The TF μ SR spectra are best described by an oscillatory function damped with a Gaussian and an oscillatory background, i.e. by

$$Gz(t) = A_0 \cos(\omega t + \varphi) e^{-\sigma^2 t^2/2} + A_{BG} \cos(\omega t + \varphi) \quad (11)$$

where $\omega = \gamma_\mu H_{int}$ is the precession frequency (H_{int} is the internal field at muon site). Solid curves in Fig. 7 are the fits of the TF μ SR spectra by the decay function in Eq. (11). In the superconducting state at $T = 0.05$ K the depolarization rate is found to increase significantly, e.g. for the TF μ SR spectra at 2.5 mT the σ increases from its value $\sigma = 0.010(2) \mu s^{-1}$ at 1.0 K to $\sigma = 1.45(4) \mu s^{-1}$ at 0.05 K. Such an increase of depolarization rate reveals bulk superconductivity in LaIrSi₃.

The maximum entropy spectra for TF μ SR precession at 1.0 K and 0.05 K are shown in Fig. 8. The maximum entropy spectra depicts the magnetic field probability distribution $P(H)$. It is clear from Fig. 8 that at

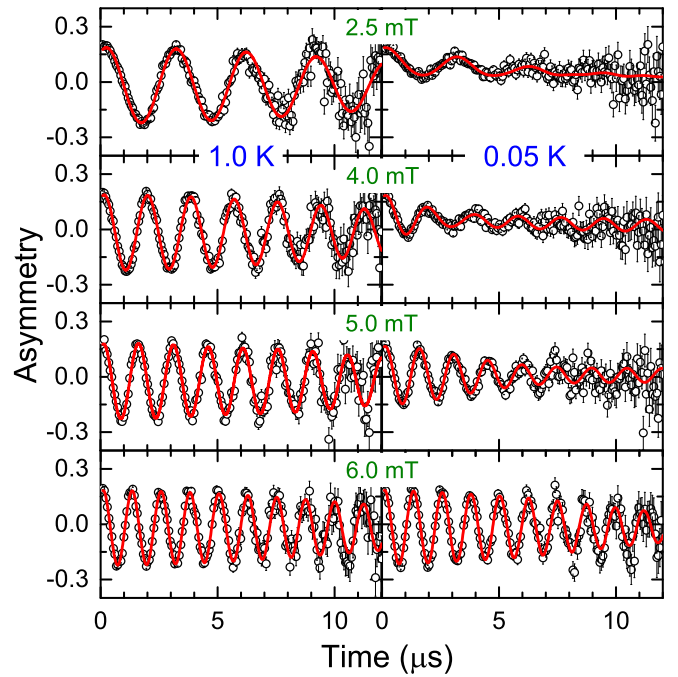


FIG. 7. (colour online) The transverse field μ SR spectra at temperatures above (1.0 K, left panels) and below (0.05 K, right panels) the superconducting T_c for indicated applied fields. The solid curves are the fits by oscillatory function in Eq. (11).

1.0 K (in normal state) sharp peaks are observed at H_{int} exactly equal to the applied H , whereas at 0.05 K (in superconducting state) one can see additional peaks. At $H = 4.0$ mT the $P(H)$ at 0.05 K shows an additional peak at $H_{int} > H$ [inset of Fig. 8]. The appearance of an additional peak (near 5.5 mT, which gives an estimation of H_c) at an internal field greater than the applied H is a characteristic of a type-I behavior and indicates a type-I superconductivity in LaIrSi₃ consistent with the above inference from the value of κ_{GL} in Table II. Further at 0.05 K for $H \leq 4.0$ mT we also observe an increase in $P(H)$ near $H_{int} \sim 0.5$ mT as is expected for a sample in Meissner state. However, no such increase in $P(H)$ is observed from Meissner volume in the intermediate state (i.e. at $H = 5.0$ mT). At $H = 6.0$ mT no additional peak is observed in $P(H)$ at $H_{int} > H$ even on expanded scale. This could be understood to be due to the fact that the applied H is close to the $H_c = 6.1$ mT (see Table II) and the sample is on the verge of transition from superconducting to normal state at $H = 6.0$ mT. Thus the μ SR data also reflect a low thermodynamic critical field $H_c \approx 5.5$ mT in line with the estimate of H_c from the heat capacity data.

VIII. CONCLUSIONS

The superconducting and normal state properties of noncentrosymmetric superconductor LaIrSi₃ which crys-

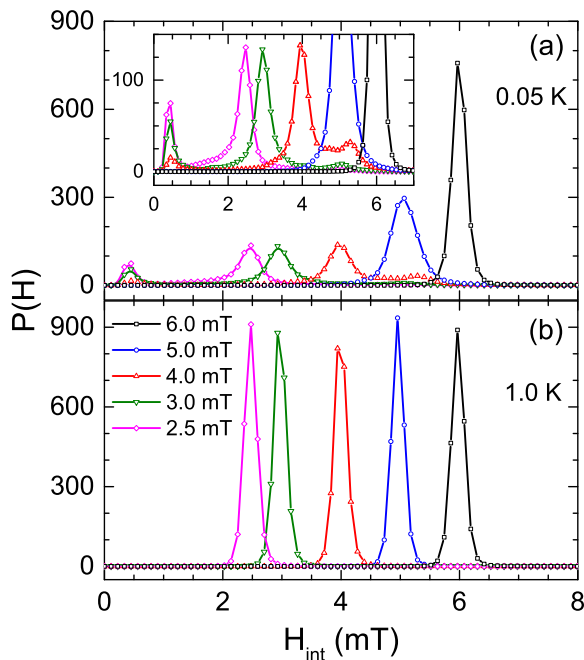


FIG. 8. (colour online) The maximum entropy spectra at different applied fields H for (a) 0.05 K, and (b) 1.0 K. Inset in (a) shows an expanded view of the magnetic field probability distribution $P(H)$.

tallizes in BaNiSn_3 -type tetragonal crystal structure (space group $I4mm$) are investigated by $C_p(T, H)$, $\rho(T, H)$ and μSR measurements which demonstrate bulk BCS superconductivity below $T_c = 0.72(1)$ K. A non-bulk superconductivity sets in at a higher T_c in $\rho(T)$. In the normal state the ρ exhibits metallic behavior and $\rho(T \geq 1.6$ K) is well described by the Bloch-Grüneisen model of resistivity. Our analysis of low temperature normal state $C_p(T)$ data yield Sommerfeld coefficient $\gamma_n = 4.60(2)$ mJ/molK² corresponding to the density of states at Fermi energy $\mathcal{D}(E_F) = 1.95(1)$ states/eV f.u. for both spin directions.

The superconducting transition is revealed by a very sharp jump in C_p at $T_c = 0.72(1)$ K however with a reduced value of $\Delta C_e/\gamma_n T_c = 1.09(3)$ than the BCS expected value of 1.43. The reduced value of $\Delta C_e/\gamma_n T_c$ seems to indicate an anisotropic energy gap in LaIrSi_3 . The superconducting state electronic heat capacity data are analyzed by single-band α -model of BCS superconductivity that describes the experimental data reasonably. The $\alpha = \Delta(0)/k_B T_c = 1.54(2)$ obtained from the jump in C_p is smaller than the $\alpha_{\text{BCS}} = 1.764$ indicating the s -wave order parameter of LaIrSi_3 to be anisotropic in momentum space. Even though the single-band α -model describes the superconducting state data reasonably, considering the split spin-up and spin-down bands in LaIrSi_3 the possibility of two-band superconductivity cannot be ruled out. Presence of two-band is also known to result in a reduced $\Delta C_e/\gamma_n T_c$.^{38,59} Since the two-band effect and anisotropy modification to single-band have similar man-

ifestations it is very difficult to distinguish between them by examining the thermodynamic quantities. Recently a two-band superconductivity with equal energy gaps was reported in SrPt_3P .⁶⁰ Further investigations are desired to check for the possibility of a similar two-band single-gap superconductivity in LaIrSi_3 .

Various normal and superconducting state parameters have been estimated which indicate a dirty limit weak-coupling type-I s -wave BCS superconductivity in LaIrSi_3 . Type-I superconductivity is further confirmed by μSR . The μSR measurement also revealed that the time-reversal symmetry is preserved in superconducting state thus confirming a conventional s -wave singlet pairing superconductivity in LaIrSi_3 . Thus despite a large splitting of Fermi surfaces due to antisymmetric coupling on account of noncentrosymmetric structure inferred from de Haas-van Alphen effect study³³ no clear signature of parity mixing or spin-triplet pairing state is found in our investigations of superconducting state properties of LaIrSi_3 .

The type-I superconductivity in LaIrSi_3 is similar to that of NCS LaRhSi_3 which also exhibits conventional s -wave electron-phonon mediated type-I superconductivity with preserved time reversal symmetry and a singlet pairing.²⁶ Both LaRhSi_3 and LaIrSi_3 have similar $\mathcal{D}(E_F)$ and Θ_D therefore one would expect the T_c of these two compounds to be similar, however we see that the $T_c = 0.72(1)$ K of LaIrSi_3 is significantly lower than the $T_c = 2.16(8)$ K of LaRhSi_3 .²⁶ While the reason for this contrasting behavior is not clear, the T_c appears to have a relation with the outer shell electronic configuration of Rh ($4d$) and Ir ($5d$) in these two superconductors. A similar trend has been observed in other $4d$ and $5d$ systems such as in LaPdSi_3 [$T_c = 2.65(5)$ K] and LaPtSi_3 [$T_c = 1.52(6)$ K] (Ref. 31) as well as in $\text{Li}_2\text{Pd}_3\text{B}$ [$T_c = 6.7$ K] and $\text{Li}_2\text{Pt}_3\text{B}$ [$T_c = 2.43$ K].¹¹ The $4d$ -based superconductors appears to have higher T_c than those having $5d$. Further investigations to understand this aspect of superconductivity in these compounds are desired.

The effect of lack of inversion symmetry on the superconducting properties of LaIrSi_3 seems not pronounced despite a large splitting of spin-up and spin-down energy bands due to ASOC. A similar behavior is reported for NCS BaPtSi_3 (Ref. 21) for which electronic-structure calculations revealed splitting of bands on account of spin-orbit interactions, however the superconductivity turned out to be conventional BCS-like with a singlet pairing. Such observations raise an important question: what else other than ASOC controls the appearance of anomalous superconducting state in a noncentrosymmetric system? The anomalous superconducting properties of the Ce-based strongly correlated NCSs, such as CePt_3Si ,⁹ CeRhSi_3 (Ref. 13) and CeIrSi_3 (Ref. 14) can naively be related to the magnetic pairing due to the presence of $4f$ moments. However, the unusual superconducting properties of weakly correlated NCSs $\text{Li}_2\text{Pt}_3\text{B}$,¹¹ LaNiC_2 ,^{19,20} and Re_6Zr (Ref. 30) are not then obvious as they do not

show any evidence of magnetic order. An important difference between the two groups of nonmagnetic NCSs, i.e. those exhibiting unusual superconducting properties and those exhibiting conventional superconductivity is the difference in their crystal structures/space groups. This may suggest that these two groups of nonmagnetic NCSs may have different Fermi surface topology that may have some role in realizing the effect of ASOC. A comparative study of extent of ASOC in nonmagnetic NCSs preferably by the technique that can directly probe Fermi surface topology, such as angle resolved photoemission spectroscopy (ARPES), complemented with band-

structure calculations can shed light on this issue and would be of help in understanding the relationship of ASOC, Fermi surface topology and anomalous superconductivity in NCSs.

ACKNOWLEDGMENTS

VKA, DTA and ADH acknowledge financial assistance from CMPC-STFC grant number CMPC-09108. AB thanks UJ and STFC for PDF funding. AMS thanks the SA-NRF (78832) and the URC of UJ for financial assistance.

* vivekkranand@gmail.com

† devashibhai.adroja@stfc.ac.uk

¹ *Non-centrosymmetric Superconductors: Introduction and Overview*, edited by E. Bauer and M. Sigrist, Lecture Notes in Physics (Springer, Berlin, 2012) Vol. 847.

² V. M. Édel'shtein, Sov. Phys. JETP **68**, 1244 (1989).

³ L. P. Gor'kov, E. I. Rashba, Phys. Rev. Lett. **87**, 037004 (2001).

⁴ K. V. Samokhin, E. S. Zijlstra, and S. K. Bose, Phys. Rev. B **69**, 094514 (2004).

⁵ P. A. Frigeri, D. F. Agterberg, A. Koga, and M. Sigrist, Phys. Rev. Lett. **92**, 097001 (2004).

⁶ S. Fujimoto, J. Phys. Soc. Jpn. **76**, 051008 (2007).

⁷ E. Bauer, G. Hilscher, H. Michor, C. Paul, E. W. Scheidt, A. Griбанov, Y. Seropegin, H. Noel, M. Sigrist, and P. Rogl, Phys. Rev. Lett. **92**, 027003 (2004).

⁸ E. Bauer, I. Bonalde, M. Sigrist, Low Temp. Phys. **31**, 748 (2005)

⁹ E. Bauer, H. Kaldarar, A. Prokofiev, E. Royanian, A. Amato, J. Sereni, W. Bramer-Escamilla, and I. Bonalde, J. Phys. Soc. Jpn. **76**, 051009 (2007).

¹⁰ K. Togano, P. Badica, Y. Nakamori, S. Orimo, H. Takeya, and K. Hirata, Phys. Rev. Lett. **93**, 247004 (2004).

¹¹ H. Q. Yuan, D. F. Agterberg, N. Hayashi, P. Badica, D. Vandervelde, K. Togano, M. Sigrist and M. B. Salamon, Phys. Rev. Lett. **97**, 017006 (2006).

¹² N. Kimura, K. Ito, K. Saitoh, Y. Umeda, H. Aoki, and T. Terashima, Phys. Rev. Lett. **95**, 247004 (2005).

¹³ N. Kimura, Y. Muro, and H. Aoki, J. Phys. Soc. Jpn. **76**, 051010 (2007).

¹⁴ I. Sugitani, Y. Okuda, H. Shishido, T. Yamada, A. Thamizhavel, E. Yamamoto, T. D. Matsuda, Y. Haga, T. Takeuchi, R. Settai, and Y. Ōnuki, J. Phys. Soc. Jpn. **75**, 043703 (2006).

¹⁵ R. Settai, I. Sugitani, Y. Okuda, A. Thamizhavel, M. Nakashima, Y. Ōnuki, and H. Harima, J. Magn. Magn. Mater. **310**, 844 (2007).

¹⁶ G. Knebel, D. Aoki, G. Lapertot, B. Salce, J. Flouquet, T. Kawai, H. Muranaka, R. Settai, and Y. Ōnuki, J. Phys. Soc. Jpn. **78**, 074714 (2009).

¹⁷ F. Honda, I. Bonalde, K. Shimizu, S. Yoshiuchi, Y. Hirose, T. Nakamura, R. Settai, and Y. Ōnuki, Phys. Rev. B **81**, 140507 (2010).

¹⁸ V. K. Pecharsky, L. L. Miller, K. A. Gschneidner, Phys. Rev. B **58**, 497 (1998).

¹⁹ A. D. Hillier, J. Quintanilla, and R. Cywinski, Phys. Rev. Lett. **102**, 117007 (2009).

²⁰ I. Bonalde, R. L. Ribeiro, K. J. Syu, H. H. Sung and W. H. Lee, New J. Phys. **13**, 123022 (2011)

²¹ E. Bauer, R. T. Khan, H. Michor, E. Royanian, A. Grytsiv, N. Melnychenko-Koblyuk, P. Rogl, D. Reith, R. Podloucky, E.-W. Scheidt, W. Wolf, and M. Marsman, Phys. Rev. B **80**, 064504 (2009).

²² T. Shibaayama, M. Nohara, H. A. Kotari, Y. Okamoto, Z. Hiroi, and H. Takagi, J. Phys. Soc. Jpn. **76**, 073708 (2007).

²³ K. Wakui, S. Akutagawa, N. Kase, K. Kawashima, T. Muranaka, Y. Iwahori, J. Abe and J. Akimitsu, J. Phys. Soc. Jpn. **78**, 034710 (2009).

²⁴ T. Klimczuk, F. Ronning, V. Sidorov, R.J. Cava, and J.D. Thompson, Phys. Rev. Lett. **99**, 257004 (2007).

²⁵ A. B. Karki, Y. M. Xiong, I. Vekhter, D. Browne, P. W. Adams, D. P. Young, K. R. Thomas, J. Y. Chan, H. Kim, and R. Prozorov, Phys. Rev. B **82**, 064512 (2010).

²⁶ V. K. Anand, A. D. Hillier, D. T. Adroja, A. M. Strydom, H. Michor, K. A. McEwen, and B. D. Rainford, Phys. Rev. B **83**, 064522 (2011).

²⁷ G. Eguchi, D. C. Peets, M. Kriener, and Y. Maeno, E. Nishibori, Y. Kumazawa, K. Banno, S. Maki, and H. Sawa, Phys. Rev. B **83**, 024512 (2011).

²⁸ P. K. Biswas, M. R. Lees, A. D. Hillier, R. I. Smith, W. G. Marshall, and D. McK. Paul, Phys. Rev. B **84**, 184529 (2011).

²⁹ A. B. Karki, Y. M. Xiong, N. Haldolaarachchige, S. Stadler, I. Vekhter, P. W. Adams, D. P. Young, W. A. Phelan, and J. Y. Chan, Phys. Rev. B **83**, 144525 (2011).

³⁰ R. P. Singh, A. D. Hillier, B. Mazidian, J. Quintanilla, J. F. Annett, D. McK. Paul, G. Balakrishnan, and M. R. Lees, Phys. Rev. Lett. **112**, 107002 (2014).

³¹ M. Smidman, A. D. Hillier, D. T. Adroja, M. R. Lees, V. K. Anand, R. P. Singh, R. I. Smith, D. M. Paul, and G. Balakrishnan, Phys. Rev. B **89**, 094509 (2014).

³² F. von Rohr, H. Luo, N. Ni, M. Wörle, and R. J. Cava, Phys. Rev. B **89**, 224504 (2014).

³³ Y. Okuda, Y. Miyauchi, Y. Ida, Y. Takeda, C. Tonohiro, Y. Oduchi, T. Yamada, N. D. Dung, T. D. Matsuda, Y. Haga, T. Takeuchi, M. Hagiwara, K. Kindo, H. Harima, K. Sugiyama, R. Settai, and Y. Ōnuki, J. Phys. Soc. Jpn. **76**, 044708 (2007).

³⁴ Y. Tada, N. Kawakami, and S. Fujimoto, Phys. Rev. B **81**, 104506 (2010).

- ³⁵ A. Thamizhavel, T. Takeuchi, T. D. Matsuda, Y. Haga, K. Sugiyama, R. Settai, and Y. Ōnuki, *J. Phys. Soc. Jpn.* **74**, 1858 (2005).
- ³⁶ P. Lejay, I. Higashi, B. Chevalier, J. Etourneau, and P. Hagenmuller, *Mater. Res. Bull.* **19**, 115 (1984).
- ³⁷ P. Haen, P. Lejay, B. Chevalier, B. Lloret, J. Etourneau and M. Sera, *J. Less-Common Met.* **110**, 321 (1985).
- ³⁸ D. C. Johnston, *Supercond. Sci. Technol.* **26**, 115011 (2013).
- ³⁹ H. Padamsee, J. E. Neighbor, and C. A. Shiffman, *J. Low Temp. Phys.* **12**, 387 (1973).
- ⁴⁰ J. Bardeen, L. N. Cooper, and J. R. Schrieffer, *Phys. Rev.* **108**, 1175 (1957).
- ⁴¹ J. Rodríguez-Carvajal, *Physica B* **192**, 55 (1993); Program Fullprof, LLB-JRC, Laboratoire Léon Brillouin, CEA-Saclay, France, 1996 (www.ill.eu/sites/fullprof/).
- ⁴² A. C. Larson and R. B. Von Dreele, *Tech. Rep. LAUR 86-748*, Los Alamos National Laboratory, 2004; B. H. Toby, *J. Appl. Cryst.* **34**, 210 (2001).
- ⁴³ N. Engel, H. F. Braun and E. Parthé, *J. Less-Common Met.* **95**, 309 (1983).
- ⁴⁴ E. Parthé, B. Chabot, H.F. Braun, and N. Engel, *Acta Crystallogr. B* **39**, 588 (1983).
- ⁴⁵ F. J. Blatt, *Physics of Electronic Conduction in Solids* (McGraw-Hill, New York, 1968).
- ⁴⁶ R. J. Goetsch, V. K. Anand, A. Pandey, and D. C. Johnston, *Phys. Rev. B* **85**, 054517 (2012).
- ⁴⁷ V. K. Anand, P. K. Perera, A. Pandey, R. J. Goetsch, A. Kreyssig, and D. C. Johnston, *Phys. Rev. B* **85**, 214523 (2012).
- ⁴⁸ C. Kittel, *Introduction to Solid State Physics*, 8th ed. (Wiley, New York, 2005).
- ⁴⁹ G. Grimvall, *Phys. Scr.* **14**, 63 (1976).
- ⁵⁰ W. McMillan, *Phys. Rev.* **167**, 331 (1968).
- ⁵¹ M. Tinkham, *Introduction to Superconductivity*, 2nd Ed. (Dover, Mineola, NY, 1996).
- ⁵² V. K. Anand, H. Kim, M. A. Tanatar, R. Prozorov, and D. C. Johnston, *Phys. Rev. B* **87**, 224510 (2013).
- ⁵³ P. G. de Gennes, *Superconductivity of Metals and Alloys* (Benjamin, New York, 1966).
- ⁵⁴ V. Moshchalkov, M. Menghini, T. Nishio, Q. H. Chen, A. V. Silhanek, V. H. Dao, L. F. Chibotaru, N. D. Zhigadlo, and J. Karpinski, *Phys. Rev. Lett.* **102**, 117001 (2009).
- ⁵⁵ D. Saint-James and P. G. de Gennes, *Phys. Letters* **7**, 306 (1963).
- ⁵⁶ M. Strongin, A. Paskin, D. G. Schweitzer, O. F. Kammerer, and P. P. Craig, *Phys. Rev. Lett.* **12**, 442 (1964).
- ⁵⁷ N. Kimura, H. Ogi, K. Satoh, G. Oshaki, K. Saitoh, H. Iida and H. Aoki, *JPS Conf. Proc.* **3**, 015011 (2014).
- ⁵⁸ T. P. Orlando, E.J. McNiff, Jr., S. Foner, and M. R. Beasley, *Phys. Rev. B* **19**, 4545 (1979).
- ⁵⁹ M. Zehetmayer, *Supercond. Sci. Technol.* **26**, 043001 (2013).
- ⁶⁰ R. Khasanov, A. Amato, P. K. Biswas, H. Luetkens, N. D. Zhigadlo, and B. Batlogg, *arXiv:1404.5473v1*.